Ultra-fine Yttria-Stabilized Zirconia for dental applications: A step forward in the quest towards strong, translucent and aging resistant dental restorations

E. Roitero, Helen Reveron, Laurent Gremillard, V. Garnier, C. Ritzberger, J. Chevalier

Ultra-fine Yttria-Stabilized Zirconia for dental applications: A step forward in the quest towards strong, translucent and aging resistant dental restorations

Published in Journal of the European Ceramic Society 43[7] pp. 2852-63 (2023)
https://doi.org/10.1016/j.jeurceramsoc.2022.07.027

E. Roitero[a,*], H. Reveron[a], L. Gremillard[a], V. Garnier[a], C. Ritzberger[b], J. Chevalier[a]

[a] Université de Lyon, INSA-Lyon, CNRS, MATEIS UMR5510, 7 Av. Jean Capelle, F-69621 Villeurbanne Cedex, France.
[b] Ivoclar Vivadent AG, Benderstrasse 2, Li-9494 Schaan, Liechtenstein
* Corresponding author: Erica.roitero@insa-lyon.fr

Keywords
Yttria-Stabilized Zirconia ; Translucency ; Nanometric ; Dental application ; Mechanical properties ; Low temperature degradation

Abstract

To decrease the light scattering caused by birefringence of the tetragonal phase of dental Yttria-Stabilized Zirconia (YSZ), two main strategies are followed: 1) increasing Y_2O_3 content to have a larger amount of non-birefringent cubic phase or 2) decreasing grain size below 100 nm to reduce their scattering coefficient. Both strategies might affect mechanical properties and aging resistance. This study shows that increasing the stabilizer content enhances both translucency and aging resistance, at the expense of mechanical properties. Nanometric-sized YSZ show, instead, very interesting compromise. Nanometric-sized zirconia stabilized with 3 mol.% of Y_2O_3 possesses high strength and toughness (above 1600 MPa and 3.3 MPa $m^{1/2}$), aging resistance and translucency, thanks to its fully-stabilized tetragonal nano-grains. Nanometric-sized zirconia stabilized with 1.5 mol.% of Y_2O_3 has the best mechanical performances (strength above 1500 MPa and toughness of 4.8 MPa $m^{1/2}$), still showing aging resistance and intermediate opacity. These results highlight the interest of moving towards Yttria-containing transformable tetragonal nano-ceramics for dental applications.

Graphical Abstract

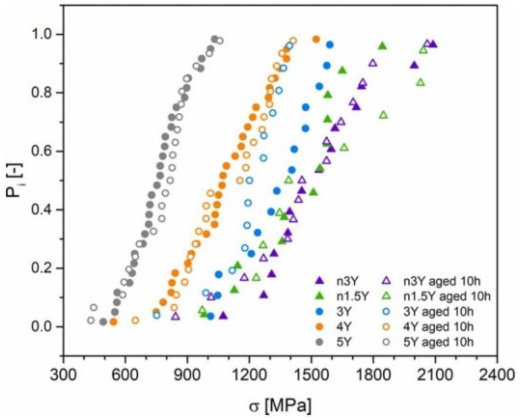

1. Introduction

Polycrystalline Tetragonal Zirconia stabilized with 3 mol.% of Yttria (3Y-TZP) has become a reference among single-oxide ceramics in dentistry [1,2], due to its good biocompatibility, resistance to corrosion, excellent mechanical properties (above 1000 MPa in bending strength and fracture toughness between 4 and 6 MPa $m^{1/2}$) [3] and good aesthetics thanks to its white color. However, in order for external restorations to meet the real-tooth appearance and because the translucency of conventional 3Y-TZP is still insufficient, veneering with a glass ceramic is often necessary. The main drawback of this bi- or multi-layered structure is its early failure due to chipping of the veneering porcelain [4]. To overcome this problem, monolithic ceramic restorations can be processed, which demand zirconia ceramics with higher translucency. The aim of new grades of Yttria-containing zirconia is, therefore, to improve translucency without unduly compromising its mechanical integrity and long term reliability [5].

3Y-TZP falls into the category of translucent ceramics, which means that light can pass through a thin slit of these materials but it will interact with its constituents so that the outcoming light is diffused, resulting in its whitish appearance. This is caused by the diffuse scattering of light on the microstructure and the defects present in the material. The main sources of this scattering in zirconia ceramics are due to differences in refractive index between [6]:

- porosity (gas trapped inside the pore) and the matrix;
- adjacent grains in birefringent crystalline structures (grains from the same tetragonal (*t*) or monoclinic (*m*) phase but with different crystallographic orientations);
- second phases (grains with different crystallographic structure than the surrounding matrix or constituted by a different material) and the matrix.

In order to increase translucency, it is necessary to reduce light scattering on one or more of these sources [7-10]. Aside from the reduction of porosity [11] and impurities, that are most often located at the grain boundaries (e.g. Al_2O_3 particles used as sintering aid in Y-TZP [12]), two other strategies help reducing scattering on grain boundaries [7,8]. The first method is to increase the content of zirconia crystallized under the cubic (*c*) phase by increasing the Yttria content above 3 mol. % [7,12,13]. The cubic symmetry is not birefringent, meaning that the refractive index is isotropic, which eliminates the scattering at the interface between cubic grains. However, YSZ materials are not fully cubic and are generally composed of both birefringent *t* and not-birefringent *c* phases, so that some scattering still happens between adjacent grains of different phases. The second method consists in decreasing the grain size (GS) of the tetragonal crystals below 100 nm to limit the scattering cross-section of the grains, as predicted by scattering models like Rayleigh-Gans-Debye [6,9,10] or Mie [9].

The two strategies mentioned above modify the microstructure (i.e. the GS), the stabilizer content and its distribution (i.e. the Yttria repartition among the constituent phases and into the grains). For zirconia ceramics this means strongly affecting mechanical properties (i.e. strength and toughness, as transformability of the tetragonal phase directly plays on stress-induced *t-m* phase transformation toughening mechanism) and its LTD resistance (i.e. influencing the metastability of tetragonal grains in steam) [13,14]. One could expect that the mechanical properties might be negatively affected due to the loss of transformation toughening, either because there is less metastable *t* phase when Yttria-content increases or because it becomes too stabilized by the reduced GS. Yet, the exact implications, challenges and benefits of playing with Yttria content and/or grain size on the compromise between mechanical properties, LTD and translucency still need clarification.

Few authors [12,17] have already reported that the increment of translucency in the so-called 'translucent zirconia' (sometimes named 'high-translucent' or 'ultra-translucent') is related to a higher yttrium content (generally spanning from 4 to 6 mol.%) and, therefore, a higher cubic phase fraction. These grades have shown an improvement in optical properties and aging resistance, but always associated to a loss in toughness and strength because of the suppression of *t-m* phase transformation toughening mechanism.

On the other hand, other authors have predicted the increment of transparency and translucency in tetragonal zirconia associated to the GS reduction below the 100 nm limit [6], [8,9,18]. However, there are only few experimental reports on the optical properties improvement of 3Y-TZP with reduced GS, usually around 50 nm [8,19,20], because of the technical difficulty of achieving fully dense materials with such small grains. Unfortunately, these works did not report on the mechanical characterization of these samples, leaving open the question about the possibility of improving optical properties in nanograined Y-TZP ceramics without affecting strength, toughness and LTD resistance. Few other studies report about zirconia with Yttria content below 3 mol.% and nanometric GS as a high toughness material [21-23] but without considering the light scattering or the optical properties. Bravo-Leon et al. [21] showed that both for nano-1YSZ and nano-1.5YSZ the indentation toughness increases with increasing GS, up to a critical GS value. They hypothesize that the condition granting the highest toughness is a very precise stabilizer/grain size combination that places the ceramic very near the phase transformation boundary, i.e. just before spontaneous transformation to the monoclinic phase occurs. The authors reported an optimized zirconia doped with 1.5 mol.% of Yttria and a GS of 110 nm (calculated with Scherrer equation from peak broadening on X-ray diffractograms) showing K_{Ic} values of 16 MPa $m^{1/2}$ (measured by indentation toughness method). In another paper, Trunec et al. [22] reported an optimized zirconia doped with 1.5 mol.% of Yttria and a GS of 85 nm (2D linear intercept method without correction, corresponding to a 133 nm real GS) showing K_{Ic} values of 15.5 MPa $m^{1/2}$ (measured by indentation toughness method) and 7.9 MPa $m^{1/2}$ (measured by chevron notched beam method). In these two papers, authors did not report about the optical properties of these tough materials nor their LTD behavior. Recently, one paper from Akhlaghi et al. [24] reported about the optical properties together with mechanical performances of fully-dense nanometric-sized YSZ doped with 1.5, 3, 6, 8 mol.% of Yttria with GS inferior to 85 nm (2D linear intercept method without correction, corresponding to a 133 nm real GS. J. Chevalier, L. Gremillard and V. Garnier, personal communication about the measuring method, 16th November 2022). Nanometric YSZ doped with 1.5 and 3 mol.% of Yttria and GS of 75 nm (2D linear intercept method without correction, corresponding to a 117 nm real GS) showed extremely high strengths (up to 2.6 GPa and 2 GPa, respectively). RIT increased with increasing Yttria content. Unfortunately, authors did not report about the LTD behavior. Paul et al. [23] described for the first time the hydrothermal aging of nanometric zirconias doped with 1.5, 2, 3 mol.% of Yttria and GS between 90 and 95 nm (2D linear intercept method with correction factor of 1.56). They reported no aging for nano-3YSZ after accelerated test in autoclave at 245 °C, 40 bar even after 14 days, while the nano-1.5YSZ completely transformed and disintegrated after just 30 min at the same conditions. They also reported a K_{Ic} of 5.1 MPa $m^{1/2}$ (measured by indentation toughness method) for the nano-1.5YSZ. In all the above-mentioned papers, the nano-1.5YSZ show a higher indentation toughness than conventional 3Y-TZP, with increasing values as the GS decreases close to the 100 nm, the critical value proposed by Bravo-Leon et al. No further mechanical or optical characterization was carried on.

These studies separately point out the potential of nanometric zirconia in terms of translucency, toughness and LTD resistance, suggesting that a better compromise of the desired properties could be achieved in these materials.

In this study, we compare the nanometric- to the submicrometric-sized YSZ with various Yttria content as strategy to increase mechanical, optical properties and LTD resistance, relating them to the different microstructural (GS) and compositional (phases and stabilizer content and distribution) features. To the best of our knowledge, no work has yet been published about the comparison of these two families of materials and no complete study encompassing mechanical, optical properties and LTD resistance of nanometric-sized YSZ zirconia has yet been reported. The objective of this study is to investigate the potential of nanometric-sized YSZ ceramics compared to submicrometric-sized YSZ in terms of compromise of physical and optical properties for possible new developments in the field of dental materials. The discussion concludes with a set of reflections summarizing the implications, issues and benefits of reducing the grain size while adapting the amount of stabilizer compared to the strategy of increasing the amount of cubic phases by increasing the Yttria content.

2. Materials and methods

2.1. YSZ ceramics

In this study two different types of Yttria Stabilized Zirconia (YSZ) ceramics provided by Ivoclar were characterized:

- Submicrometric-sized YSZ doped with 3, 4 and 5 mol.% of Yttria (referred to as 3Y, 4Y and 5Y, respectively). Commercial powders from Tosoh (Japan) with particle size around 100 nm were employed (TZ-PX245, TZ-PX524, TZ-PX430 for 3Y, 4Y and 5Y, respectively). The starting powders contained 0.05 wt% of Al_20_3. Samples were produced by slip-casting on a plaster mold and then sintered in an air furnace at 1500 °C for 2 h (heating rate of 10 °C/min up to 900 °C, 30 min dwell at 900 °C and then heating rate of 3 °C/min up to 1500 °C). A pre-sintering cycle was added to bar samples at 900 °C for 2 h (heating rate of 1 °C/min).

- Nanometric-sized YSZ doped with 1.5 and 3 mol.% of Yttria (referred to as n1.5Y and n3Y, respectively). Colloidal suspensions of nanozirconia in water (particles size of 10–20 nm and containing 0.25 wt% and 0.7 wt% of Al_20_3 for n3Y and n1.5Y, respectively) were transformed into formable gels via osmotic processing. The starting suspensions (50–60 wt% loading) were concentrated to form a gel in the following manner: 50–200 g of suspension were placed in a semi-permeable tubular membrane (Spectra/Par dialysis membrane MWCO 6000–8000) and closed with clips. The loaded membrane was then immersed in a 10–20 wt% polyethylene glycol–water solution in a closed container placed on a shaking table (at 100 rpm for 12–24 h). A translucent and soft gel was obtained, with 70–80 wt% solid loading. The gels were shaped into discs or bars with CIP and let dry at 23 °C at constant relative humidity of 50% during 10 days. The green bodies were pre-sintered using a multi-segment heating cycle at temperatures between 300 °C and 400 °C (dwell time of 2 h). For each heating segment, the heating rate varied from 0.4 to 5.0 °C/h. Samples were then sintered in an air furnace at 1100 °C for 2 h (heating rate of 10 °C/min).

It is to note that samples were not manufactured out of commercial Ivoclar products. Submicrometric-sized YSZ were prepared with the uncolored base materials of their commercial products (*e.g.* IPS e.max ZirCAD) and compared to the uncolored nanometric-sized YSZ, which are not yet commercialized.

Samples were in the form of discs (12.5 ± 0.5 mm in diameter and 1.1 ± 0.1 mm thick) and bars (with a squared section of 3 × 3 mm^2 and 22–23 mm long). One of the circular surfaces of discs and one of the rectangular surfaces of bars were ground and polished with diamond suspensions down to 1 µm. If no further preparation was done before analysis, the samples will be labelled in the 'as-received' state.

2.2. Microstructure and phase composition

The polished surface of the samples was imaged with a Scanning Electron Microscope (SEM-Zeiss SUPRA VP55) equipped with Secondary Electrons (SE) detector. The surface of the nanometric-sized YSZ samples were further polished with a 6 keV Ar^+ ion beam at a 6° off-normal incidence (Gatan Ilion II) for 5 min. Additional surface treatments (thermal and chemical etching and coating of conductive layer) were avoided and the surfaces were imaged directly at low accelerating voltages (1–2 kV). This allowed imaging the top layer of grains on the surface without introducing artefacts and the contrast between grains with different crystallographic orientations was obtained thanks to electron channeling. The average GS and its distribution were calculated by the linear intercept method (the 2D linear intercept values measured on the micrographs were multiplied by a factor of 1.56 to get the average 3D GS, according to the ASTM E 112 standard [25]). Density of samples was calculated by Archimedes' method with water as the buoyant medium.

To determine the crystalline phases nature and to quantify their relative amount, the polished surface of samples was analyzed with X-ray Diffraction (XRD) using a Bragg-Brentano symmetric geometry. The analysis was performed on a diffractometer (Bruker, D8-Advance) using Cu K_α radiation (40 kV and 40 mA). Two sets of diffractograms were recorded: a complete diffractogram $20° < 2\theta < 145°$ at a scan rate of 0.02 s/step and a step size of 0.019° for performing Rietveld refinement and a diffractogram focused on $27° < 2\theta < 33°$ at a scan rate of 1.5 s/step and a step size of 0.03° for the determination of the volume fraction of the monoclinic phase (V_m) by using Garvie and Nickolson [26] (Eq. 6) and Toraya [27] equations (Eq. 7). The complete diffractograms were recorded on the 'as received' samples and on the same samples after an annealing thermal treatment in air (at 1100 °C for 20 min for the submicrometric-sized grains grades and at 1000 °C for 15 min for the nanometric-sized grains). The goal of this annealing step is to eliminate any residual stresses near the surface generated during polishing and to allow a more precise analysis of lattice parameters from the Rietveld refinement of more symmetric peaks. The crystallographic parameters and relative amount of zirconia phases were determined from the Rietveld refinement performed with the Topas 4.0 software (Bruker, Germany). The average Yttria content inside each zirconia polymorph was evaluated thanks to an empirical equation relating the lattice parameters of the cubic and tetragonal phases to the Yttria molar content (expressed as mol. % of $YO_{1.5}$). The equations [28,29] employed for the tetragonal phase are the following:

$a_t = 0.00377\, YO_{1.5} + 5.0785$ (Eq.1)
And $c_t = -0.00290\, YO_{1.5} + 5.1925$ (Eq.2)
And for the cubic phase: $a_c = 0.00173\, YO_{1.5} + 5.1132$ (Eq. 3)

2.3. Mechanical properties

The biaxial strength was tested on disc samples (12.5 ± 0.5 mm in diameter and 1.1 ± 0.1 mm thick) with the piston on three balls method, according to the ISO 6872 standard for dental ceramics [30]. The polished surface of the disc was placed under biaxial tensile stress and the load versus displacement curve was recorded until disc failure on a universal testing machine (Model 8562, Instron, USA). At least 15 discs were tested for each grade. Discs breaking not in the center or with anomalous features in the load-displacement curves were not considered in the analysis. A Weibull statistic was applied to the results to model the strength distribution and determine the characteristic strength (σ_0), the Weibull modulus (m) [31,32] and their confidence intervals [33].

The size of the critical defect (a circular defect of radius a_{critic} right below the surface) was calculated from the measured values of mean strength and K_{Ic} as described in [34].

Toughness was measured on bars (with a squared section of 3 × 3 mm^2 and 22–23 mm long) by the Single Edge V-Notch Beam (SEVNB) method, which is preferred to indentation-based toughness evaluation: a sharp notch was produced on the side of a test bar up to a total depth of 750 ± 125 µm. It consists of a pre-notch (550 ± 75 µm deep) made with a diamond saw followed by a shallow sharp notch (200 ± 50 µm deep) produced by ultra-short pulsed femto-laser ablation (UPLA) [35]. An annealing thermal treatment, as the one done before XRD analysis, was performed before the mechanical test, so that the residual stresses and phase transformation eventually produced during notch manufacturing were released and did not affect the toughness measurement. The bar was then placed under tensile stress with a 4-point bending setup in displacement control mode (0.5 mm/min) and the load versus displacement curve was recorded until failure on a universal testing machine (Model 8562, Instron, USA). The toughness K_{Ic} was then calculated with the following equations [35]:

$$K_{Ic} = \frac{3F(S_1 - S_2)}{2bw^2} Y\sqrt{a} \quad \text{(Eq.4)}$$

$$\text{Where } Y = \frac{1.1215\sqrt{\pi}}{\beta^{3/2}} \left[\frac{5}{8} - \frac{5}{12}\alpha + \frac{1}{8}\alpha^2\beta^6 + \frac{3}{2}\exp\left(-\frac{6.1342\alpha}{\beta}\right)\right]$$

S_1 and S_2 are the outer and inner spans of the 4 point bending setup, b is the thickness, w the width, F the applied load, a the crack length, $\alpha = a/w$ and $\beta = 1 - \alpha$. Three samples per grade were tested.

XRD was performed on the fracture surface of the tested bars for the nanometric-sized YSZ, to investigate potential stress-induced transformation. The volume fraction of the monoclinic phase (V_m) at the fracture surface was calculated by using Garvie and Nickolson [26] and Toraya [27] equations.

2.4. Low temperature degradation

The LTD kinetics was followed during a series of accelerated aging tests in saturated water vapor in an autoclave at 134 °C and 2 bars, up to 200 h (this long accelerated aging time was applied in order to follow the kinetics of nanometric-sized zirconia until saturation). In order to follow the transformation kinetics, three samples per grade were placed in the autoclave and the progression of the transformation was followed by estimating the transformed volume fraction of monoclinic phase (V_m) by XRD at different time points. The amount of monoclinic

phase was calculated from the equation proposed by Toraya [27], an empirical relation that allows to calculate the volume fraction of monoclinic phase (V_m) as a function of the intensity ratio (X_m), as follows:

$$V_m = \frac{1.311X_m}{1+0.311X_m} \qquad \text{(Eq. 6)}$$

The intensity ratio is calculated as $X_m = \frac{[I_m(-111)+I_m(111)]}{[I_m(-111)+I_m(111)]+I_t(111)}$ (Eq. 7), where I is the area of the peak on the normalized diffractogram of the tetragonal (suffix t) and monoclinic (suffix m) phases, according to Garvie and Nicholson equation [26].

The biaxial strength was measured on samples aged 10 h in autoclave, which for 3Y-TZP roughly corresponds to 20–40 years in vivo conditions [36,37], in order to ensure that mechanical properties are maintained. The results were treated statistically with one-way analysis of variance (ANOVA) with a significance level $\alpha = 0.05$, in order to investigate statistical differences in the mean values between 'as received' and artificially aged materials.

2.5. Optical properties

The optical properties of the different materials were measured in a UV–vis spectrophotometer (Jasco Y-670, France), equipped with an integrating sphere with 60 mm diameter. The Real In-line Transmittance (*RIT*), the Total Forward Transmittance (T_{tot}) and the Total Reflectivity (R_{tot}) were recorded as a function of wavelength in the visible range (from 350 nm to 800 nm). The tested samples were discs employed for mechanical testing, their thickness was reduced by grinding to 1 ± 0.02 mm and both surfaces were polished with diamond suspension down to 1 μm.

The Contrast Ratio (*CR*) and Opalescence (*OP*) were calculated from the *CIELAB* parameters with the following equations, according to the DIN EN ISO 11664 [38] and BS 5612 [39] standards:

$$CR = \frac{Y_b}{Y_w} \qquad \text{(Eq. 8)}$$

And

$$OP = ((a_T^* - a_R^*)^2 + (b_T^* - b_R^*)^2)^{1/2} \text{ (Eq. 9)}$$

where Y_b is the luminance measured from the reflectance spectrum of the sample on a black background, Y_w is the luminance measured from the reflectance spectrum of the sample on a white background, and a^* and b^* are the color coordinates in the CIELAB system, measured from reflectance (suffix R) and transmittance (suffix T) spectra. The CR gives an indication of the opacity/translucency, it ranges from 0 (total translucency) to 1 (total opacity).

3. Results

SEM images of the microstructures of the different grades of zirconia are presented in Fig. 1 along with their GS distributions.

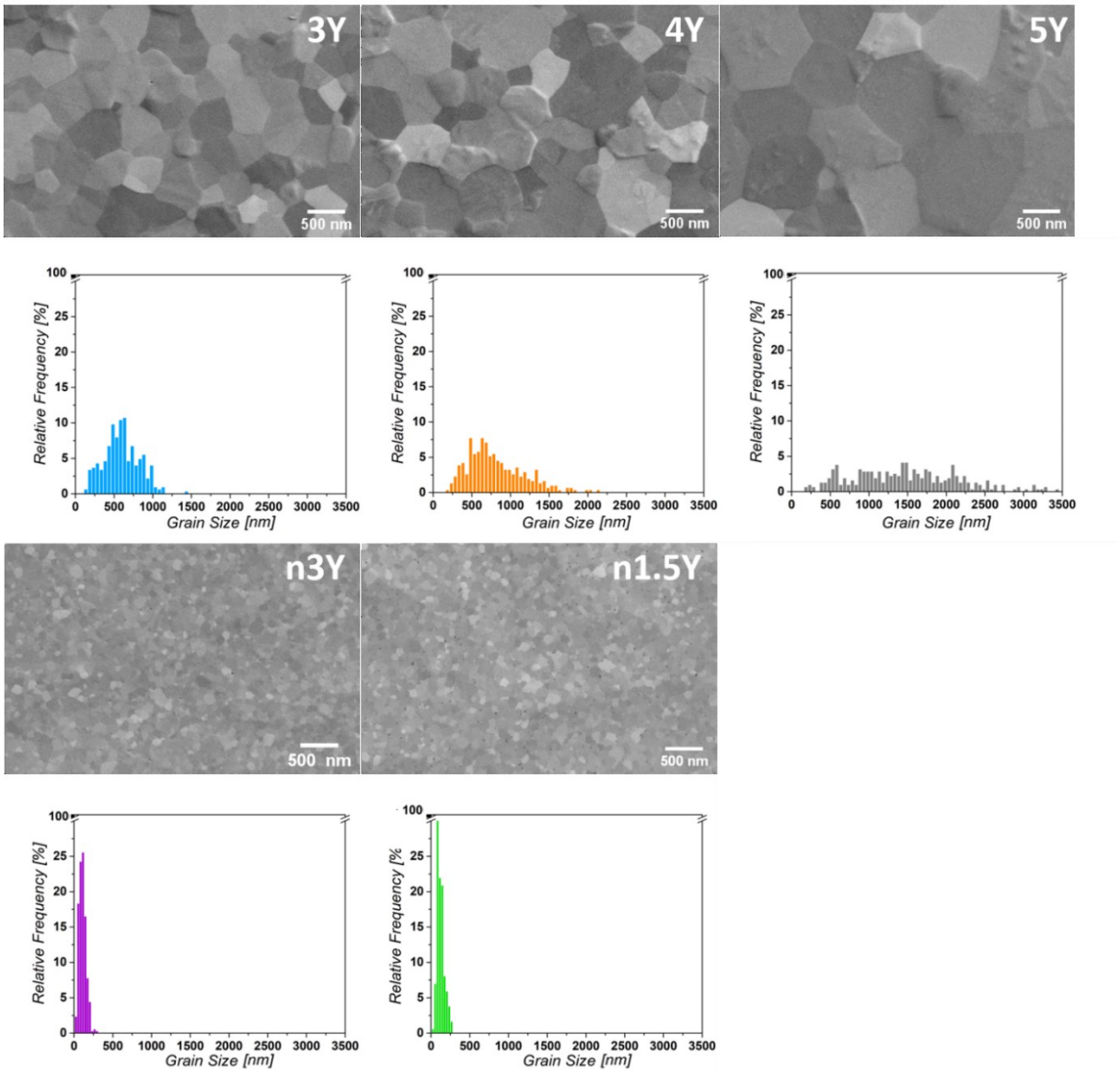

Figure 1 : SEM images of different zirconia grades and related GS distributions. Some nanoporosity (small black spots on the micrographs) can be observed on the surfaces of the nanometric-sized grades, especially in n1.5Y.

The mean value and standard deviation of the GS distributions as well as the final density are summarized in Table 1. The microstructure is homogeneous on all the surfaces observed and for all the grades. The GS of 3Y corresponds to a standard 3YTZP. In the sub-micrometric grades, the GS increases with Y content and the distributions are likely bimodal or even multimodal, becoming larger as Y content increases. Both nanometric-sized zirconias have a much smaller GS and a very narrow monomodal GS distribution.

Table 1: Grain Size and density of the zirconia grades of this study (note that the grain size reported is the real grain size, i.e. the 2D linear intercept multiplied by a 1.56 factor).*

Sample	GS* ± SD [nm]	Density [g·cm^{-3}]
3Y	596 ± 223	6.09 ± 0.00
4Y	810 ± 368	6.04 ± 0.00
5Y	1480 ± 710	6.06 ± 0.01
n1.5Y	125 ± 47	6.06 ± 0.02
n3Y	111 ± 44	6.03 ± 0.02

No second phase, in terms of isolated alumina grain inclusions, was observed with SEM for all grades. Since the reported solubility of alumina in zirconia is extremely limited [40], and since no distinct alumina grains were observed in the microstructures of all grades of material investigated in this work, it is reasonable to suppose that aluminum cations are distributed at the grain boundaries, as suggested in prior works [41,42].

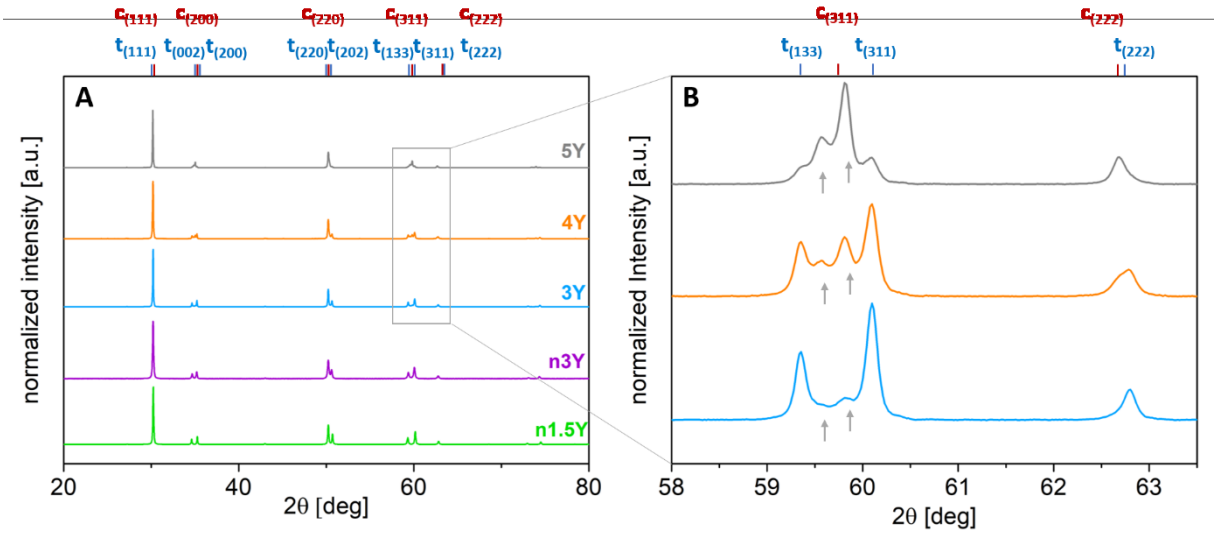

Figure 2 : X-ray diffractograms of different zirconia grades after thermal annealing treatment. (A) complete diffractograms and (B) selected zone for submicrometric-sized ceramics, where t and c peaks are clearly visible (peaks belonging to the distorted cubic phase are marked with gray arrows). Nanometric-sized zirconias do not display such separated t and c reflections since the amount of c phase is almost negligible.

The X-ray diffractograms after the annealing thermal treatment of the 5 grades are reported in Fig. 2. As expected and commonly reported in the literature, the three submicrometric-sized grades present both the tetragonal and the cubic phases' diffraction peaks [2], with the cubic reflections becoming more intense with increasing Yttria content. However, it is interesting to observe that the so-called cubic phase shows doublets instead of the single peaks corresponding to the reflections of a perfectly cubic structure [14]. For instance, this can be observed in the range of $59° < 2\theta < 60°$ (see Fig. 2B), where the cubic and tetragonal reflections do not overlap and it is more evident in the 5Y and 4Y grades because of the larger amount of cubic phase and their more intense reflections. Those reflections can be attributed, instead, to a slightly distorted cubic lattice, closer to the tetragonal symmetry. This structure has been previously reported in the literature as 'pseudo cubic' or 'distorted cubic' phase or even 'tetragonal prime' (t′) [15,43,44]. In this paper, we will refer to this phase as 'distorted cubic' since it has a lower tetragonality (e.g. $c/a = 1.007$ versus $c/a = 1.016$ for the tetragonal phase in 3Y, as summarized in Table 2) and it is richer in Yttria (e.g. 5.95 mol.% versus 2.57 mol.% for the tetragonal phase in 3Y, as summarized in Table 2). Therefore, the 'distorted cubic' phase is less prone to

transformation into monoclinic phase, being closer to a cubic phase than the 'normal' tetragonal phase both in terms of tetragonality and higher stabilizer content. The 'distorted cubic' phase is the result of a diffusion-less transformation of the *c* phase (stable at the sintering temperature) during 'fast' cooling: if the diffusion of Y^{3+} is not fast enough to increase the stabilizer content to *c* phase equilibrium concentration at lower temperatures, the cubic phase transforms to the 'distorted cubic', or t′, instead [43]. For the nanometric-sized grades, the main constituent of the samples after the annealing treatment is the tetragonal phase (i.e. 99.7 wt% in n1.5Y and 97.5 wt% in n3Y, as shown in Table 2), as already observed for this combination of stabilizer content/grain size [21,22]. Nevertheless, other peaks could almost completely overlap with those of the tetragonal phase, making it very difficult to establish whether this second phase is a cubic or a distorted cubic since both phases provided a good fit in the Rietveld refinement. For simplicity, we employed a cubic phase as the second constituent for the Rietveld refinement calculations performed on n1.5Y and n3Y samples.

Table 2 : Phase composition and crystallographic parameters of the zirconia grades (results from the Rietveld analysis).

				distorted cubic				*tetragonal*			
grade	Y_2O_3 *(mol%)*	***c* phase** (wt. %)	***t* phase** *(wt. %)*	a_c (Å)	c_c (Å)	c_c/a_c	Y_2O_{3c} (mol %)	a_t (Å)	c_t (Å)	c_t/a_t	Y_2O_{3t} (mol %)
3Y	3	18.8	81.2	5.123	5.158	1.007	5.9	5.098	5.178	1.016	2.6
4Y	4	39.7	60.3	5.125	5.157	1.006	6.1	5.099	5.177	1.015	2.7
5Y	5	74.8	25.2	5.127	5.155	1.005	6.4	5.101	5.175	1.015	3.0
				cubic				*tetragonal*			
grade	Y_2O_3 *(mol%)*	***c* phase** (wt. %)	***t* phase** *(wt. %)*	a_c (Å)		Y_2O_{3c} (mol %)		a_t (Å)	c_t (Å)	c_t/a_t	Y_2O_{3t} (mol %)
n1.5Y	1.5	0.3	99.7	1.535		6.4		5.091	5.183	1.018	1.7
n3Y	3	2.5	97.5	5.136		6.7		5.102	5.174	1.014	3.1

The amount and crystallographic characteristics of each phase, estimated from the Rietveld analyses, are summarized in Table 2. In the sub-micrometric grades, the amount of distorted cubic phase increases with the Yttria content, as predicted by the Zirconia-Yttria phase diagram [28], [45]. The tetragonality of the distorted cubic lattice is much lower than the tetragonal phase in all the grades, confirming that this structure is closer to a cubic symmetry than to a tetragonal one. The amount of Yttria in the tetragonal and distorted cubic phases is slightly different among grades and it is higher, in both phases, in the 5Y than in the 3Y and 4Y. Furthermore, the Yttria content in the tetragonal phase of 3Y and 4Y is lower than 3 mol.% (2.6 mol.% and 2.7 mol.%, respectively), below the commonly recognized stabilization limit of the tetragonal phase, because of phase partitioning [43] and its segregation inside the distorted cubic phase. On the other hand, the tetragonal phase in n1.5Y and n3Y contains the nominal 1.5 mol.% and 3 mol.% respectively, as suggested by the Rietveld analysis.

The biaxial strength distributions of the as-received samples and the samples after an accelerated autoclave-aging treatment of 10 h are presented in Fig. 3 and the associated mechanical properties are summarized in Table 3.

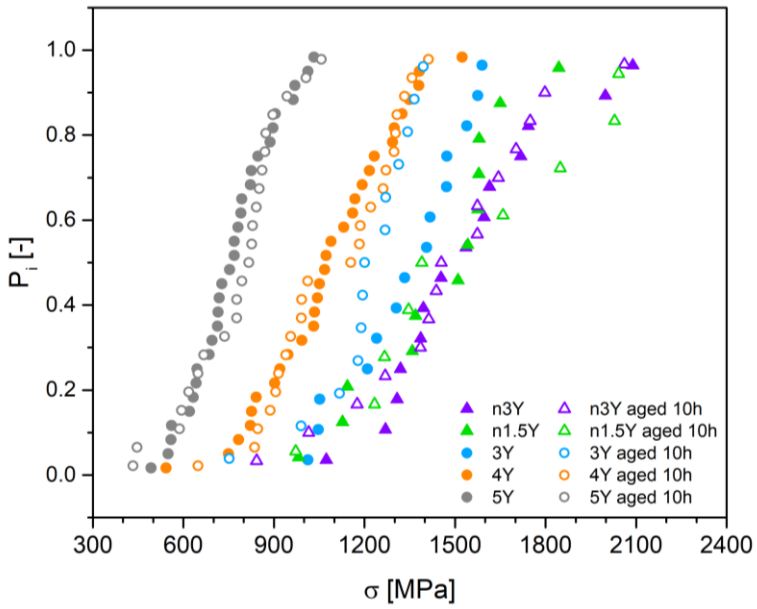

Figure 3 : Weibull plot of the biaxial strength of the different zirconia grades for the (filled symbols) as-received samples and (hollow symbols) 10 h autoclave-aged samples.

Table 3. Summary of the mechanical properties of the different zirconia grades. Mean biaxial strength (σ_{mean}), characteristic strength (σ_0), Weibull modulus (m) for the as-received and 10 h autoclave-aged samples, and the monoclinic volume fractions (V_m) after 10 h of accelerated aging in autoclave, toughness (K_{Ic}) measured by SEVNB method on the as-received samples and critical defect size (a_{critic}).

Sample	σ_{mean}	σ_{mean} aged 10 h	σ_0 [CI 95%]	σ_0 aged 10 h [CI 95%]	m [CI 95%]	m aged 10 h [CI 95%]	V_m aged 10 h	K_{Ic} by SEVNB	a_{critic}
	[MPa]	[MPa]	[MPa]	[MPa]	[-]	[-]	[%]	[MPa $m^{1/2}$]	[µm]
3Y	1334	1198	1424 [1266–1576]	1278 [1136–1414]	7.7 [4.5–12,3]	7.1 [4.2 – 11.4]	49	3.8 ± 0.1	4.4
4Y	1079	1096	1167 [1076–1257]	1184 [1091–1274]	5.6 [3.8–7.8]	6.0 [4.1 – 8.4]	18	3.1 ± 0.1	4.0
5Y	759	772	816 [752–878]	836 [771–900]	6.5 [4.4–9.1]	5.3 [3.6 – 7.4]	0	2.2 ± 0.1	3.5
n1.5Y	1438	1532	1545 [1375–1711]	1561 [1389–1728]	6.5 [3.8–10.4]	4.7 [2.7 – 7.5]	9	4.8 ± 0.4	4.4
n3Y	1473	1536	1649 [1466–1825]	1606 [1428 – 1778]	6.6 [3.8–10.4]	5.3 [3.1 – 8.5]	0	3.3 ± 0.3	1.8

For the submicrometric zirconias, both the mean value of the biaxial strength distribution and the characteristic strength of the associated Weibull distribution decrease with increasing Yttria content. The nanometric grades show very high values of strength, reaching around 1500 MPa. The Weibull modulus and its confidence intervals are similar for all the grades.

The effect of the accelerated aging treatment on the mechanical properties is not significant for 4Y, 5Y, n3Y and n1.5Y grades, as it can be observed from the almost overlapping strength distributions of the as-received samples and the aged ones, in Fig. 3, and as confirmed with an ANOVA test. For the 3Y grade, the strength distribution of the aged samples is slightly shifted

towards lower values. However, the ANOVA test pointed out that at $\alpha = 0.05$ the difference in strength between the two distributions is not yet significant ($p = 0.071$). Monoclinic phase was detected with XRD on the surface of the 10 h aged 3Y (V_m = 49 ± 5%, see Table 3). The transformation front and associated microstructural damages may just have reached enough depth so that they start to interfere with existing defects close to the surface or that they become a critical defect themselves, slightly reducing the strength. It is important to point out that, for the 3Y grade, 10 h at these accelerated test conditions (saturated water vapor at 134 °C and 2 bars) are equivalent to around 20–40 years at 'in vivo' conditions [37], therefore, this is still a very reasonable duration before any sign of strength degradation appears.

The fracture toughness measured with the SEVNB method for each grade is reported in Table 3. K_{Ic} increases with decreasing Yttria content, for submicrometric grades. By calculating the size of the critical defect (a circular defect of radius a_{critic} right below the surface [34]) from the measured values of mean strength and K_{Ic} (see Table 3) we observe that they are very similar for the three grades, corroborating the fact that the difference in strength between the submicrometric grades comes from the difference in their toughness and not from their defect populations, i.e. processing. Nanometric grades show interestingly high values of toughness: n3Y has a slightly lower K_{Ic} than 3Y, while n1.5Y has by far the highest value of the tested materials. These results are in agreement with those previously reported for a similar material in Ref. [22].

The optical images of the fracture surfaces of the tested bars of the nanometric-sized samples are shown in Fig. 4A and B for n3Y and n1.5Y, respectively. At this magnification, the fracture surface of n3Y is almost flat without asperities (and consistent to what is observed for conventional grade, i.e. submicrometric-sized YSZ), while the fracture surface of n1.5Y is peculiar, with rough and clear river marks. In Fig. 4C, the diffractograms show that on the surface of n1.5Y, monoclinic phase is detected (peaks marked with asterisks) associated to stress-induced transformation, while on n3Y's only *t* phase peaks are observed.

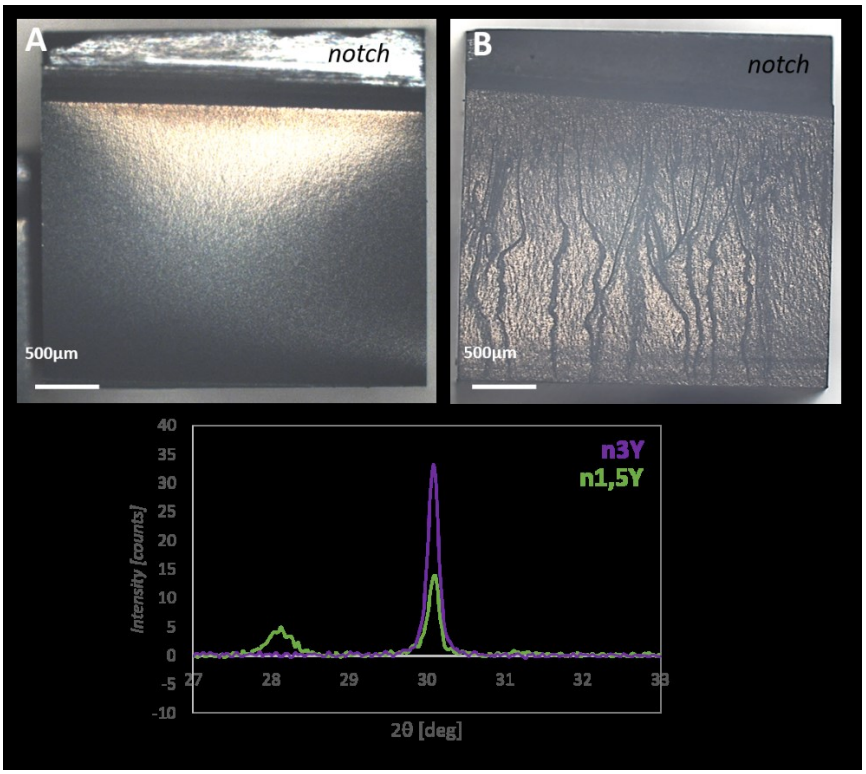

Figure 4 : Fracture surfaces of the nanometric-sized grades' bars tested with SEVNB method, (A) n3Y and (B) n1.5Y, respectively. In (C), the diffractograms recorded on these fracture surfaces, showing the presence of m-phase peaks (marked with asterisks) on the surface of n1.5Y.

The LTD kinetics (in autoclave at 134 °C and 2 bars) are presented in Fig. 5 up to 200 h of accelerated test. All the grades have no trace of monoclinic phase ($V_{m\,0} = 0\%$) before starting aging tests except for n1.5Y ($V_{m,0} \approx 3.5\%$). During accelerated tests, on the surface of n1.5Y, n3Y, 3Y and 4Y it was possible to detect some monoclinic phase whose content increased over test duration, showing that these grades all undergo LTD. However, the final amount of monoclinic phase reached at the saturation plateau is much higher for the submicrometric than the nanometric grained ceramics. On the other hand, it was not possible to detect any monoclinic phase on the surface of the 5Y after 200 h of accelerated aging, confirming that this grade does not undergo spontaneous *t-m* transformation even after these very long treatments. 3Y and 4Y grades start showing traces of monoclinic phase since the first steps of the accelerated tests, so that the *t-m* transformation in these grades starts immediately at these conditions. Both grades reach surface saturation detectable by XRD ($V_{m\,max} \approx 75\%$ for 3Y and $V_{m\,max} \approx 48\%$ for 4Y) around the same time (50 h of accelerated test). On the surface of n1.5Y the amount of monoclinic phase starts to increase since the beginning of the accelerated tests too, while for the n3Y there is an incubation period (up to 30 h of accelerated test) before any phase transformation could be detected. n3Y reaches a plateau ($V_{m\ max} \approx 3.5\%$) almost immediately after the detection of the transformation. In the n1.5Y the amount of monoclinic phase does not seem to reach a plateau but, instead, it increases very slowly in a stepwise manner up to a maximum (low value) of $V_{m,max} \approx 10\%$ after 200 h of accelerated aging test.

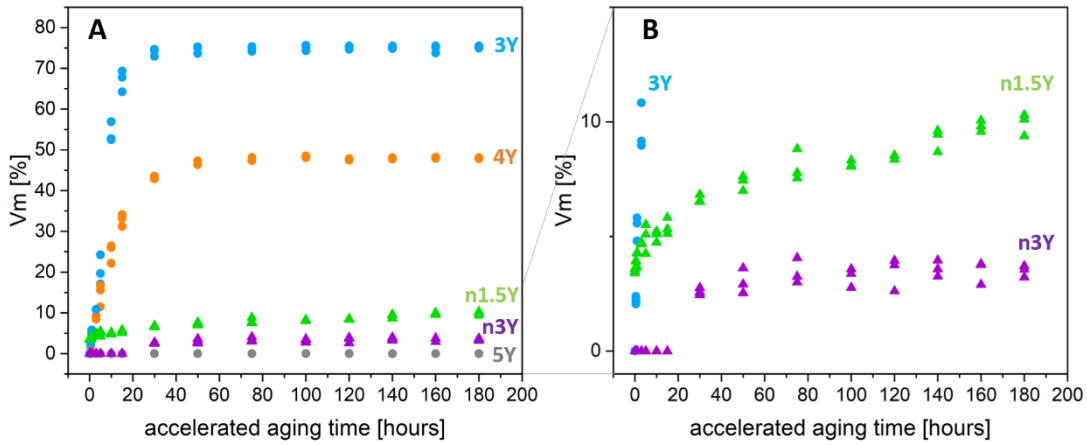

Figure 5 : (A) LTD kinetics of the different zirconia grades and (B) a magnification of the kinetics of the nanometric-sized grains for the accelerated test in autoclave at 134 °C and 2 bars.

The optical properties are summarized in Fig. 6, where the *RIT* (Real In-line Transmission, i.e. transparency) and the T_{tot} (the total transmission, consisting of the in-line transmission together with diffuse transmission, i.e. translucency) are plotted against the wavelength, for the entire visible spectrum. The CR and OP of the different grades are summarized in Table 4. Among the submicrometric grades, 3Y and 4Y have very similar translucency while 5Y has higher *RIT*, especially in the yellow-red portion of the spectrum, contributing to a slightly higher T_{tot}. The *CR* of the three grades decreases as the stabilizer content increases, while their *OP* is not significantly different except for 5Y, which is higher thanks to its better transparency in the red range of the spectrum. The nanometric grades have different optical properties from the submicrometric grades: they are both more transparent at longer wavelengths than at shorter wavelengths, i.e. they have a more pronounced slope in the RIT and T_{tot} curves, resulting in higher opalescence. n3Y has the highest RIT among all grades, especially in the yellow-red portion of the spectrum (reaching a transparency of almost 35% at 800 nm). However, its T_{tot} is higher than micrometric grades' only for longer wavelengths, so that the overall translucency

does not vary significantly, as it can be seen from the similar values of *CR* (see Table 4). n1.5Y has a transparency close to that of 5Y, however, its T_{tot} is lower than all the other grades and its CR is the highest (the opaquest material).

Sample	CR	OP
3Y	0.55	6.20
4Y	0.51	6.70
5Y	0.46	7.58
n1.5Y	0.63	11.20
n3Y	0.51	12.40

Table 4. Summary of the optical properties. Contrast ratio (CR) and Opalescence (OP).

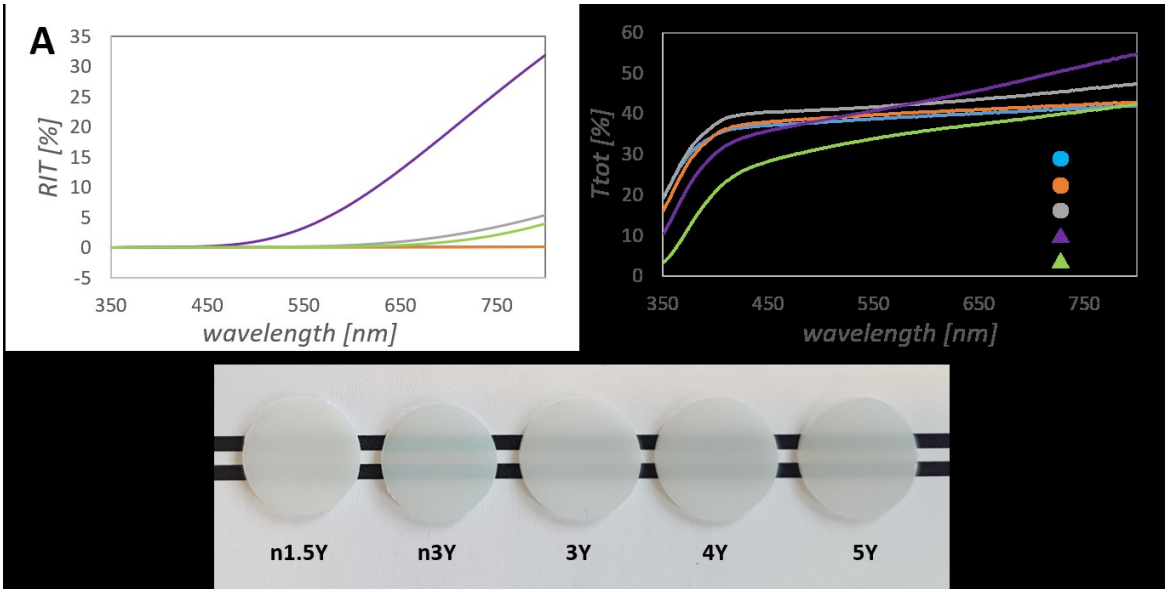

Figure 6 : Optical properties of the different zirconia grades. (A) Real In-line Transmission as a function of wavelength, (B) Total Forward Transmission as a function of wavelength and (C) optical images of 1 mm thick samples.

4. Discussion

4.1. Effect of Yttria content on the transformability and LTD of the tetragonal phase

The variation of all the properties described so far for the submicrometric grades is ruled by their phase composition, their grain size and the amount of stabilizer in each phase, which can lead to a more or less transformable tetragonal phase [43]. It is well known [45,46] that both toughness, strength, but also LTD, are directly correlated to the ability of the tetragonal phase to transform into monoclinic, upon the application of a local stress and the diffusion of water-derived species in the crystalline network of YSZ mediated by the presence of oxygen vacancies, respectively. In general, the lower the toughness (i.e. the lower the transformability of the metastable *t* phase) the better the LTD resistance. This is the case for 5Y, which does not show any sign of phase transformation even after 200 h of accelerated test in autoclave at 134 °C (see Fig. 5) and has the lowest toughness and mean strength among studied grades (2.2 MPa $m^{1/2}$ and 760 MPa respectively). The 4Y grade, that is generally considered as less transformable than 3Y compositions because of its higher Yttria content, exhibits a similar propensity to LTD. Normalizing the aging kinetics curves by the maximum transformed volume fraction reached at the plateau ($V_{m,max}$) in each sample (monoclinic volume fraction, $f_m = V_m/V_{m,max}$), it is possible to observe that the curves of 3Y and 4Y are extremely close (see Fig.

7). Degradation starts immediately after exposure to hydrothermal conditions. Their rates of transformation are very similar and the main difference between the two materials is the maximum monoclinic volume fraction reached at the transformation plateau. This is because, in 4Y, the tetragonal phase does not contain enough stabilizer (2.7 mol.% of Y_2O_3 according to Rietveld analysis, see Table 2) to be non-transformable. Its composition is, instead, very similar to that of the tetragonal phase in 3Y (2.6 mol.% of Y_2O_3 according to Rietveld analysis, see Table 2) and this is the reason for their very similar normalized LTD kinetics. It is interesting to notice that also the 5Y grade contains some tetragonal phase (≈ 25 wt%) but with a higher Yttria content (3.0 mol.%), which is enough to fully stabilize the phase, as confirmed by the lack of phase transformation during accelerated aging tests. It is, therefore, the amount of stabilizer in the tetragonal phase that defines its transformability and not the total nominal stabilizer content.

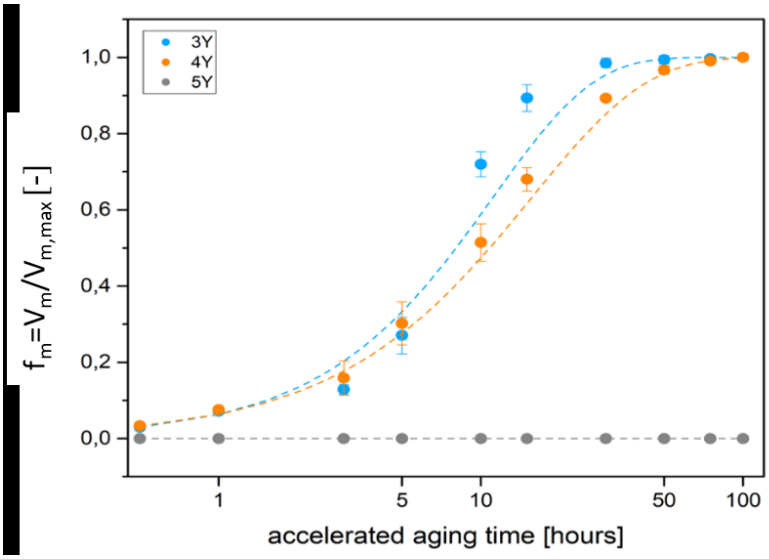

Figure 7 : Normalized LTD kinetics curves for the submicrometric grades.

The reason of the non-homogeneous distribution of Yttrium can be attributed to phase partitioning in the *c-t* region during the dwell time at 1500 °C, followed by a fast cooling that do not allow Y^{3+} redistribution according to thermodynamic equilibrium of the phase diagram [45]. The cubic (or distorted-cubic or non-transformable tetragonal) phase is richer in Yttria and it can deplete the stabilizer content of the neighboring tetragonal grains at these sintering conditions [43]. Another reason could be a non-homogeneous content and/or distribution of stabilizer inside the starting powder particles [47]. If the stabilizer content is homogeneously distributed in the starting powder, then phase partitioning should be the main reason for Yttria redistribution among phases and the sintering thermal cycle (temperature and dwell time) determines the local stabilizer content and the transformability of the tetragonal phase. Therefore, it is important to remember that for the submicrometric grades the nominal content of Yttria exceeding the stabilization limit may not be sufficient to ensure LTD resistance and that the sintering cycle characteristics can affect the tetragonal phase stability.

The maximum monoclinic volume fraction reached at the plateau for 3Y and 4Y is $V_{m,max} \approx 75\%$ and $V_{m,max} \approx 48\%$, respectively. The weight fraction of the *t* phase calculated with the Rietveld analysis is 81.2% in 3Y and 60.3% in 4Y, corresponding to a volume fraction of 81.1% and 60.1%, respectively. For 3Y, these values agree well, suggesting that nearly the entire tetragonal transformable phase available has undergone phase transformation under aging conditions. For 4Y, the majority of *t* phase has transformed under aging conditions but, even though a plateau has been reached, a fraction of it did not transform. This may be because a small fraction of the

t phase still have enough Y_2O_3 to be fully stable, since the Y_2O_3 content estimated with the Rietveld refinement (2.7 mol.%) is the average of higher and lower values of stabilizer insider different tetragonal grains.

For submicrometric grades, the presence of (distorted) cubic phase due to the sintering cycle in the *c-t* biphasic region is the responsible of Yttria depletion inside the neighboring tetragonal grains and their ability to transform. On the other hand, since nanometric grades are practically monophasic and fully tetragonal since they are sintered at lower temperature, these grades should be less prone to phase partitioning.

4.2. Effect of the grain size and the balance between grain size and Yttria content on the mechanical and optical properties of YSZ ceramics stabilized with 3 mol.% of Yttria

It is interesting to compare the performances of n3Y and 3Y: these two grades have the same nominal Yttria content but n3Y shows a much finer microstructure (GS ≈ 110 nm versus ≈ 600 nm, respectively) and different phases arrangement and composition (due to phase partitioning for the conventional 3Y and not for the n3Y), resulting in a very different properties combination. n3Y has a significantly higher mean flexural strength (1473 MPa and 1334 MPa for n3Y and 3Y, respectively and according to an ANOVA test at $\alpha = 0.05$ with $p = 0.038$), better LTD resistance (almost no transformation before 30 h of accelerated test at 134 °C) and a much higher transparency (RIT at 800 nm of ≈30% and ≈0.2% for n3Y and 3Y, respectively). Only the toughness is slightly lower in n3Y than in conventional 3Y (3.3 ± 0.3 MPa $m^{1/2}$ and 3.8 ± 0.1 MPa $m^{1/2}$, for n3Y and 3Y respectively). One of the reasons of the reduction of toughness could be the absence of the transformation toughening mechanisms in n3Y because of the full stabilization of the tetragonal phase. The hypothesis of non-transformability of the nanometric tetragonal grains in n3Y is corroborated by the almost negligible amount of monoclinic phase detected after accelerated aging tests, that could involve only few grains not fully stabilized. Moreover, tetragonal grains in n3Y are richer in Yttria and have a smaller tetragonality (1.014 versus 1.016 in 3Y). This alone could explain the non-transformability of the tetragonal phase. However, it is well known [45,48-50] that also the GS is a factor affecting the stabilization of the tetragonal phase and that there exist a critical GS below which *t-m* transformation is suppressed. Garvie [49] claimed first that for nanometric powders of pure zirconia this critical crystallite size exists because of the dominant role of surface energy in nanometer-sized particles (balance between chemical and surface energy [45,49,51,52]). The exact value of this critical size is not unique since it depends on the temperature, the dopant type and concentration, the type of synthesis of particles and their surface chemistry, the presence of applied or internal stresses and/or strain (further explanations can be found in Refs. [45,48]). Typically, critical crystallite size for pure zirconia powders in the range 20–30 nm have been reported [49,52,53]. The existence of critical crystallite size for powders evidences the role of surface energy in the stabilization of zirconia phases. In the case of polycrystalline materials, were the crystallites are surrounded by other grains, this critical crystallite size would not depend on solid-gas surface energy anymore, but on grain boundaries energy, instead. For materials with the same nominal Y concentration as n3Y and 3Y, the larger grain boundary specific surface of ultrafine n3Y than 3Y's is the main reason for the complete stabilization of the *t* phase.

Finally, also the presence of a higher amount of Al_2O_3 in n3Y (0.05 wt% in 3Y and 0.25 wt% and n3Y) may have an impact on the LTD kinetics since Al_2O_3 is known to improve the resistance to LTD of YSZ [42,54,55]. However, since Al^{3+} (or Al'_{Zr} if we employ Kröger-Vink notation) tend to segregate at grain boundaries [42,56] both in submicrometric- and nanometric-

sized zirconia [41], and no secondary phase particles were observed in the microstructures, it is reasonable to suppose that all the cations will be distributed along grain boundaries in both materials. The dopant concentration at the grain-boundary do not correspond to the nominal dopant content: it will, instead, depend on the grain boundary density (S_v), i.e. the amount of grain boundary surface per unit volume. S_v is, in turn, inversely proportional to the GS (S_v can be calculated as a function of the 2D mean lineal intercept, $\bar{l} = \frac{GS}{1.56}$, as $S_v = \frac{2}{\bar{l}}$ [25]). The grain boundary density in the nanometric-sized ceramic is 5 times higher than in the submicrometric-size, as is the nominal amount of Al_2O_3. Therefore, under the hypothesis that Al'_{Zr}segregates at grain boundaries in both materials, the concentration of cations at the grain boundary should be virtually the same for n3Y and 3Y. It seems, therefore, reasonable to imagine that the effect of alumina additions may be very similar in both materials.

The increment of RIT in n3Y, observed especially at longer wavelengths (see Fig. 6), is in agreement with previous observations by Klimke et al. [9] and can be explained with Mie scattering model by the reduced scattering on grain boundaries thanks to the smaller scattering cross-section of the nano-grains. It is important, also, to point out that the tetragonality of n3Y is smaller than 3Y, so that its birefringence should also be smaller, further contributing to the increment in transparency. This results in both a higher translucency and opalescence, that bring n3Y's optical properties closer to that of natural enamel [13].

4.3. Effect of the balance between grain size and Yttria content on the mechanical properties and LTD resistance of n1.5YSZ

Comparison of the n3Y with the n1.5Y helps shedding more light on the transformability, or not, of the nano-grains. The n1.5Y ceramic shows the best combination of strength and toughness among the tested samples, together with a very good LTD resistance (less than 10% of monoclinic volume fraction after 200 h at 134 °C). This is in contrast with common behavior of Yttria-stabilized zirconia ceramics, which are limited by the trade-off between toughness and aging resistance. To understand the origin of this interesting behavior, the criteria of transformability of the nanometric tetragonal grains doped with 1.5 mol.% of Yttria must be further understood. As it can be observed in Fig. 4A and 4B, the fracture surface of the n1.5Y looks completely different than the n3Y's, being rougher and presenting clear river marks converging towards the fracture origin at the laser notch. The specific fracture surface area of the n1.5Y is much larger than n3Y's and it has a higher amount of monoclinic phase on it, detectable with XRD as indicated in the diffractogram in Fig. 4C. These observations, together with the high value of toughness, suggest that n1.5Y undergoes phase transformation upon stress application. This means that the tetragonal phase of n1.5Y is highly transformable upon stress application, as one could expect from the low amount of stabilizer (1.7 mol.% from Rietveld analysis) and its high tetragonality 1.018. This particular combination of GS and stabilizer content is considered to be right below the phase transformation boundary mentioned by Bravo-Leon [21], that should grant the highest stress-induced transformability. It is surprising, though, to observe that the highly transformable tetragonal phase is not susceptible to a more severe LTD. The explanation for the retardation of the aging rate of YSZ ceramics could be found in the defect structure of zirconia grain boundary and the influence of both the reduced GS and the dopant concentration on the Oxygen vacancies ($V_O^{\cdot\cdot}$, if we employ Kröger-Vink notation) distribution at grain boundaries [41,42]. A grain-boundary defect structure model proposed by Guo for YSZ [57] consists of depletion and solute enrichment (i.e. substitutional Y^{3+} and Al^{3+}, or Y'_{Zr} and Y'_{Al} if we employ Kröger-Vink notation, in YSZ) in the space-charge layers around the grain boundary core. Nanometric-sized materials have a much higher grain boundary density so that solute segregation at grain boundaries becomes more

important. In YSZ with GS around 100 nm this is accompanied by further $V_O^{\cdot\cdot}$ depletion in the space-charge layers [58]. The lower amount of vacant sites available for the diffusion of water-derived species, that should be filled to trigger the transformation at the grain boundaries, may slow down the kinetics of the transformation in humid environments [57,59,60].

On the other hand, the presence of a higher amount of Al_2O_3 in n1.5Y than n3Y (0.7 wt% and 0.25 wt%, respectively) may have an impact on the LTD kinetics since Al_2O_3 is known to improve the resistance to LTD of YSZ [42,54,55]. These two grades have similar GS (125 nm for n1.5Y and 111 nm for n3Y), so that their grain boundary density S_v is also comparable. Under the hypothesis that Al'_{Zr} segregates at grain boundaries in both materials, its concentration at grain boundaries should be higher in n1.5Y than in n3Y (3 times higher, according to the nominal amount of Al_2O_3) and that can further contribute to the LTD retardation in n1.5Y since it has been proven that only Al'_{Zr} segregated at the grain boundary has a retarding effect on the LTD of YSZ [54].

n1.5Y is the grade with the highest opacity (see Fig. 6 and Table 4) in spite of the presence of nanograins with a GS comparable to the more translucent n3Y. This can be explained by the more important scattering because of the higher tetragonality associated to a larger birefringence and, also, by the presence of nanoporosity, which was by far the highest among the studied grades, as it can be seen in the micrographs in Fig. 1. This nanoporosity is a source of backscattering [11]: if it is further reduced, the opacity of this grade could be decreased, making it a very interesting candidate with all the desired properties for aesthetic dental applications.

4.4. Nanometric zirconia: a better place in the trade-off between mechanical, optical and LTD resistance properties?

In Fig. 8 the properties of all grades characterized in this study are summarized to simplify their comparison in terms of compromise between the mechanical, optical and LTD resistance properties. As depicted in the graph in Fig. 8A, the grades with higher toughness are also those with higher strength: nanometric YSZ and 3Y are the grades that exhibit the best mechanical performances, with n1.5Y showing an exceptionally high combination of these properties (1438 MPa and 4.8 MPa $m^{1/2}$). In particular, the best mechanical performances belong to the ceramics that are mainly composed of transformable *t* phase, which is responsible of the activation of phase-transformation toughening mechanisms, as n1.5Y and 3Y. A direct comparison of the mechanical performances of the materials studied here with the literature is difficult. Only one paper [24] reports biaxial strength measurements of nanometric-sized YSZ doped with 1.5 and 3 mol.% of Yttria with similar GS (2.6 GPa and 2 GPa, respectively). Besides, toughness was never measured by SEVNB in the small corpus of articles dealing with nanometric sized YSZ. However, a similar trend as the one found in the literature was found here, with increasing toughness when decreasing the yttria content at comparable grain size (as in the case of n1.5Y and n3Y) and when increasing the grain size at comparable dopant content (as in the case of 3Y and n3Y).

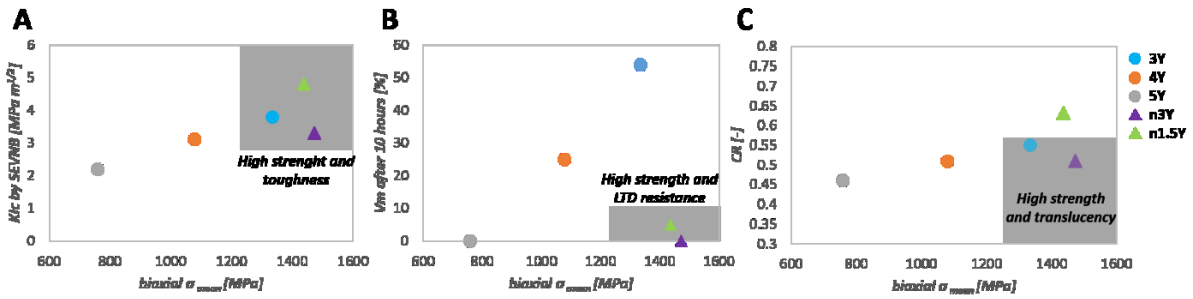

Figure 8 : Summary of the mechanical, optical and LTD resistance properties of the zirconia grades. In (A) the compromise between strength and toughness, in (B) the compromise between strength and LTD resistance and in (C) the compromise between strength and optical properties.

The balance between mechanical properties and aging resistance can be deduced from Fig. 8B: submicrometric YSZ are more resistant to aging as the stabilizer content is increased at the expense of strength and toughness. On the other hand, nanometric grades show the best compromise between these two properties and are the only ones having both high strength and very small LTD. In n1.5Y this is possible thanks to the highly transformable *t* phase of the nanograins, that are, however, resistant to *t-m* transformation in humid environment due to the lower amount of oxygen vacancies in the space-charge layer of nanograins and the presence of Al_2O_3. The extremely high LTD resistance in n3Y is granted by the fully stabilized *t* phase of the nanograins.

Finally, the balance between opacity and mechanical properties is shown in Fig. 8C: for submicrometric grades the CR (i.e. opacity) is reduced as the less birefringent distorted cubic fraction is increased by adding more stabilizer, at the expense of mechanical properties. Again, n3Y shows the best compromise (reduced opacity because of the less sensitivity of the nanograins to birefringence) while n1.5Y shows the highest opacity of all the grades tested, even though only slightly worse than 3Y, because of its high tetragonality and birefringence and the presence of residual nanoporosity. The effect of Al_2O_3 content on optical properties has not been taken into account in this study since no precipitated particles were observed in all grades, so that scattering on secondary phases could be ruled out.

Thus, the best trade-off between mechanical, optical and LTD resistance properties turns toward nanometric ceramics because they combine the advantage of nanograins' lower sensitivity to birefringence to good mechanical properties and LTD resistance. Nevertheless, there is still a lot to understand about their toughening mechanisms and resistance to LTD.

5. Conclusions

Two strategies to produce more translucent YSZ have been directly compared: submicrometric-sized YSZ with higher stabilizer content to increase the fraction of less-birefringent distorted cubic phase versus nanometric-sized YSZ with lower stabilizer content to decrease the scattering coefficient of birefringent tetragonal nanograins. Both have been proven effective in producing less opaque ceramics, however, the comparison of LTD resistance, mechanical and optical properties, shows that nanometric-sized materials offer a better compromise of performances and are, therefore, well-suited for applications in dentistry. The processing of nanometric-sized YSZ is more complex and time-consuming than conventional powder processing of submicrometric-sized YSZ, especially for the osmotic processing steps. However, the manufacturing of dental restorations based on a nanometric-sized YSZ is feasible, but it will strongly depend on the final products. For instance, the CAD/CAM milling process is possible, but the milling strategy should be adapted to get reliable dental restorations, which fits to the need of the patients.

The performances of submicrometric-sized YSZ are controlled by the trade-off between translucency and resistance to LTD, on one hand, and mechanical properties, on the other hand. In 5Y, by increasing the fraction of fully stabilized distorted *c* phase up to 74.8 wt% and the amount of stabilizer in the *t* phase up to 3 mol.%, both transformation toughening mechanisms and water-mediated *t-m* transformation are suppressed. Light scattering is reduced thanks to the larger fraction of less birefringent distorted-cubic phase.

n3Y with a GS of 111 ± 44 nm is composed of non-transformable tetragonal nanograins and shows the best compromise among the desired properties. This microstructure shows a very high LTD resistance but also the suppression of transformation-toughening mechanisms. Even though this grade has slightly lower toughness than transformable tetragonal n1.5Y and 3Y, its strength is still extremely high. Its translucency and transparency at longer wavelengths are the highest among the studied ceramics, thanks to a combination of reduced birefringence of its *t* phase with lower tetragonality and a reduced scattering coefficient thanks to the ultrafine GS.

n1.5Y with a GS of 125 ± 47 nm is composed of highly transformable tetragonal nanograins, showing that the combination of ultrafine GS and lower stabilizer content does not completely stabilize the *t* phase. Thanks to the activation of transformation toughening mechanisms, n1.5Y has the best mechanical properties compromise and it is still resistant to LTD, thanks to the lower amount of oxygen vacancies in the space-charge layer of nanograins and the addition of Al_2O_3 slowing down water-derived species diffusion in the lattice. This properties combination was not yet shown by any other YSZ material. Therefore, the strategy of decreasing GS below 100 nm together with decreasing Y-content in order to have a microstructure with transformable nanograins seems very promising.

Declaration of Competing Interest

The authors declare the following financial interests/personal relationships which may be considered as potential competing interests: Erica Roitero reports financial support was provided by IVOCLAR.

Acknowledgements

The authors would like to acknowledge the CLYM (Centre Lyonnais de Microscopie: www.clym.fr) for providing access to their microscopy facilities. The study has been funded and the samples processed and provided by IVOCLAR. Special thanks to Yijun (Adrian) Wang, Ph.D. and Wei Xu, Ph.D. for their help in the process of the samples and for fruitful discussions and to Pablo Moreno and his team at Grupo de Aplicaciones del Láser y Fotónica (ALF), Universidad de Salamanca for the femto-laser machining.

References

[1] I. Denry and J. Kelly, "State of the art of zirconia for dental applications.," *Dent. Mater.*, vol. 24, no. 3, pp. 299–307, Mar. 2008, doi: 10.1016/j.dental.2007.05.007.

[2] J. Kelly and I. Denry, "Stabilized zirconia as a structural ceramic: an overview.," *Dent. Mater.*, vol. 24, no. 3, pp. 289–98, Mar. 2008, doi: 10.1016/j.dental.2007.05.005.

[3] M. Turon-Vinas and M. Anglada, "Strength and fracture toughness of zirconia dental ceramics," *Dent. Mater.*, vol. 34, no. 3, pp. 365–375, 2018, doi: 10.1016/j.dental.2017.12.007.

[4] E. D. Rekow, N. R. F. a Silva, P. G. Coelho, Y. Zhang, P. Guess, and V. P. Thompson, "Performance of dental ceramics: challenges for improvements.," *J. Dent. Res.*, vol. 90, no. 8, pp. 937–52, Aug. 2011, doi: 10.1177/0022034510391795.

[5] Y. Zhang and B. R. Lawn, "Novel Zirconia Materials in Dentistry," *J. Dent. Res.*, vol. 97, no. 2, pp. 140–147, 2018, doi: 10.1177/0022034517737483.

[6] A. Krell, J. Klimke, and T. Hutzler, "Transparent compact ceramics : Inherent physical issues," *Opt. Mater. (Amst).*, vol. 31, no. 8, pp. 1144–1150, 2009, doi: 10.1016/j.optmat.2008.12.009.

[7] S. F. Wang *et al.*, "Transparent ceramics: Processing, materials and applications," *Prog. Solid State Chem.*, vol. 41, pp. 20–54, 2013, doi: 10.1016/j.progsolidstchem.2012.12.002.

[8] Y. Zhang, "Making yttria-stabilized tetragonal zirconia translucent," *Dent. Mater.*, vol. 30, no. 10, pp. 1195–1203, 2014, doi: 10.1016/j.dental.2014.08.375.

[9] J. Klimke, M. Trunec, and A. Krell, "Transparent Tetragonal Yttria-Stabilized Zirconia Ceramics : Influence of Scattering Caused by Birefringence," *J. Am. Ceram. Soc.*, vol. 1858, no. 94, pp. 1850–1858, 2011, doi: 10.1111/j.1551-2916.2010.04322.x.

[10] R. Apetz and M. P. B. Van Bruggen, "Transparent Alumina : A Light-Scattering Model," *J. Am. Ceram. Soc.*, vol. 86, no. 3, pp. 480–486, 2003.

[11] I. Yamashita and K. Tsukuma, "Light scattering by residual pores in transparent zirconia ceramics," *J. Ceram. Soc. Japan*, vol. 119, pp. 133–135, 2011.

[12] F. Zhang *et al.*, "Strength, toughness and aging stability of highly-translucent Y-TZP ceramics for dental restorations," *Dent. Mater.*, vol. 32, no. 12, pp. e327–e337, 2016, doi: 10.1016/j.dental.2016.09.025.

[13] E. Camposilvan *et al.*, "Aging resistance, mechanical properties and translucency of different yttria-stabilized zirconia ceramics for monolithic dental crown applications," *Dent. Mater.*, vol. 34, no. 6, pp. 879–890, 2018, doi: 10.1016/j.dental.2018.03.006.
[14] F. Zhang, H. Reveron, B. C. Spies, B. Van Meerbeek, and J. Chevalier, "Trade-off between fracture resistance and translucency of zirconia and lithium-disilicate glass ceramics for monolithic restorations," *Acta Biomater.*, vol. 91, pp. 24–34, 2019, doi: 10.1016/j.actbio.2019.04.043.
[15] A. Harada *et al.*, "Mechanical and microstructural properties of ultra-translucent dental zirconia ceramic stabilized with 5 mol% yttria," *J. Mech. Behav. Biomed. Mater.*, vol. 111, no. April, 2020, doi: 10.1016/j.jmbbm.2020.103974.
[16] E. N. S. de Araújo-Júnior *et al.*, "Ultra-translucent zirconia processing and aging effect on microstructural, optical, and mechanical properties," *Dent. Mater.*, vol. 38, no. 4, pp. 587–600, 2022, doi: 10.1016/j.dental.2022.02.016.
[17] G. K. R. Pereira, L. F. Guilardi, K. S. Dapieve, C. J. Kleverlaan, M. P. Rippe, and L. F. Valandro, "Mechanical reliability, fatigue strength and survival analysis of new polycrystalline translucent zirconia ceramics for monolithic restorations," *J. Mech. Behav. Biomed. Mater.*, vol. 85, no. May, pp. 57–65, 2018, doi: 10.1016/j.jmbbm.2018.05.029.
[18] W. Pabst and S. Hříbalová, "Light scattering models for describing the transmittance of transparent and translucent alumina and zirconia ceramics," *J. Eur. Ceram. Soc.*, vol. 41, no. 3, pp. 2058–2075, 2021, doi: 10.1016/j.jeurceramsoc.2020.10.025.
[19] S. R. Casolco, J. Xu, and J. E. Garay, "Transparent/translucent polycrystalline nanostructured yttria stabilized zirconia with varying colors," *Scr. Mater.*, vol. 58, no. 6, pp. 516–519, 2008, doi: 10.1016/j.scriptamat.2007.11.014.
[20] B. U. Anselmi-tamburini, J. N. Woolman, and Z. A. Munir, "Transparent Nanometric Cubic and Tetragonal Zirconia Obtained by High-Pressure Pulsed Electric Current Sintering **," pp. 3267–3273, 2007, doi: 10.1002/adfm.200600959.
[21] A. Bravo-Leon, Y. Morikawa, M. Kawahara, and M. J. Mayo, "Fracture toughness of nanocrystalline tetragonal zirconia with low yttria content," *Acta Mater.*, vol. 50, no. 18, pp. 4555–4562, 2002, doi: 10.1016/S1359-6454(02)00283-5.
[22] M. Trunec and Z. Chlup, "Higher fracture toughness of tetragonal zirconia ceramics through nanocrystalline structure," *Scr. Mater.*, vol. 61, no. 1, pp. 56–59, 2009, doi: 10.1016/j.scriptamat.2009.03.019.
[23] A. Paul, B. Vaidhyanathan, and J. G. P. Binner, "Hydrothermal Aging Behavior of Nanocrystalline Y-TZP Ceramics," vol. 2152, no. 28476, pp. 2146–2152, 2011, doi: 10.1111/j.1551-2916.2010.04341.x.
[24] O. Akhlaghi *et al.*, "Transparent high-strength nanosized yttria stabilized zirconia obtained by pressure-less sintering," *J. Eur. Ceram. Soc.*, vol. 42, pp. 7187–7195, 2022, doi: 10.1016/j.jeurceramsoc.2022.07.027.
[25] A. International, "ASTM E112-12 - Standard Test Methods for Determining Average Grain Size," *ASTM Int.*, vol. E112-12, pp. 1–27, 2012, doi: 10.1520/E0112-12.1.4.
[26] R. Garvie and P. Nicholson, "Phase analysis in zirconia systems," *J. Am. Ceram. ...*, no. June, pp. 303–305, 1972, doi: 10.1111/j.1151-2916.1972.tb11290.x.
[27] H. Toraya, M. Yoshimura, and S. Somiya, "Calibration Curve for Quantitative Analysis of the Monoclinic-Tetragonal ZrO2 System by X-Ray Diffraction.," *Commun. Am. Ceram. Soc.*, vol. 67, no. June, pp. C119–C121, 1984, doi: 10.1111/j.1151-2916.1984.tb19715.x.
[28] H. Scott, "Phase relationships in the zirconia-yttria system," *J. Mater. Sci.*, vol. 10, pp. 1527–1535, 1975, Accessed: Aug. 19, 2014. [Online]. Available: http://link.springer.com/article/10.1007/BF01031853.

[29] C. Wei and L. Gremillard, "Towards the prediction of hydrothermal ageing of 3Y-TZP bioceramics from processing parameters," *Acta Mater.*, vol. 144, pp. 245–256, 2018, doi: 10.1016/j.actamat.2017.10.061.
[30] "ISO 6872:2008 Dentistry-Ceramic materials." 2008.
[31] R. Danzer, W. Harrer, P. Supancic, T. Lube, Z. Wang, and A. B??rger, "The ball on three balls test-Strength and failure analysis of different materials," *J. Eur. Ceram. Soc.*, vol. 27, no. 2–3, pp. 1481–1485, 2007, doi: 10.1016/j.jeurceramsoc.2006.05.034.
[32] W. Weibull, "A statistical distribution function of wide applicability," *Journal of applied mechanics*, vol. 18. pp. 293–297, 1951, doi: citeulike-article-id:8491543.
[33] I. J. Davies, "Confidence limits for Weibull parameters estimated using linear least squares analysis," *J. Eur. Ceram. Soc.*, vol. 37, no. 15, pp. 5057–5064, 2017, doi: 10.1016/j.jeurceramsoc.2017.05.051.
[34] R. Danzer, "On the relationship between ceramic strength and the requirements for mechanical design," *J. Eur. Ceram. Soc.*, vol. 34, no. 15, pp. 3435–3460, 2014, doi: 10.1016/j.jeurceramsoc.2014.04.026.
[35] M. Turon-Vinas and M. Anglada, "Fracture toughness of zirconia from a shallow notch produced by ultra-short pulsed laser ablation," *J. Eur. Ceram. Soc.*, vol. 34, no. 15, pp. 3865–3870, 2014, doi: 10.1016/j.jeurceramsoc.2014.05.009.
[36] S. Deville, L. Gremillard, J. Chevalier, and G. Fantozzi, "A Critical Comparison of Methods for the Determination of the Aging Sensitivity in Biomedical Grade Yttria-Stabilized Zirconia," *J. Biomed. Mater. Res. - Part B Appl. Biomater.*, vol. 72, no. 2, pp. 239–245, 2004, doi: 10.1002/jbm.b.30123.
[37] J. Chevalier, B. Cales, and J. M. Drouin, "Low-Temperature Aging of Y-TZP Ceramics," *J. Am. Ceram. Soc.*, vol. 54, pp. 2150–2154, 1999.
[38] "DIN EN ISO 11664-4 Colorimetry – Part 4: CIE 1976 L*a*b* Colour space." 2012.
[39] "BS 5612 : 1978 Specifications for Dental Porcelains for jacket crowns." 1978.
[40] A. Z. Yttria, S. M. Lakiza, and L. M. Lopato, "Stable and Metastable Phase Relations in the System," vol. 902, no. 193020, pp. 893–902, 1997.
[41] X. Guo and R. Waser, "Electrical properties of the grain boundaries of oxygen ion conductors : Acceptor-doped zirconia and ceria," *Prog. Mater. Sci.*, vol. 51, pp. 151–210, 2006, doi: 10.1016/j.pmatsci.2005.07.001.
[42] F. Zhang *et al.*, "Highly-translucent, strong and aging-resistant 3Y-TZP ceramics for dental restoration by grain boundary segregation," *Acta Biomater.*, vol. 16, no. 1, pp. 215–222, 2015, doi: 10.1016/j.actbio.2015.01.037.
[43] D. Bučevac, T. Kosmač, and A. Kocjan, "The influence of yttrium-segregation-dependent phase partitioning and residual stresses on the aging and fracture behaviour of 3Y-TZP ceramics," *Acta Biomater.*, vol. 62, pp. 306–316, 2017, doi: 10.1016/j.actbio.2017.08.014.
[44] T.-S. Sheu, T.-Y. Tien, and I.-W. Chen, "Cubic-to-Tetragonal (t') Transformation in Zirconia-Containing Systems," *J. Am. Ceram. Soc.*, vol. 75, no. 5, pp. 1108–1116, 1992, doi: 10.1111/j.1151-2916.1992.tb05546.x.
[45] J. Chevalier, L. Gremillard, A. V. Virkar, and D. R. Clarke, "The Tetragonal-Monoclinic Transformation in Zirconia: Lessons Learned and Future Trends," *J. Am. Ceram. Soc.*, vol. 92, no. 9, pp. 1901–1920, Sep. 2009, doi: 10.1111/j.1551-2916.2009.03278.x.
[46] A. Della Bona and J. Kelly, "The clinical success of all-ceramic restorations," *J. Am. Dent. Assoc.*, vol. 139, no. suppl 4, 2008, Accessed: Dec. 16, 2013. [Online]. Available: http://www.jada.info/content/139/suppl_4/8S.short.
[47] F. Zhang, B. Van Meerbeek, and J. Vleugels, "Importance of tetragonal phase in high-translucent partially stabilized zirconia for dental restorations," *Dent. Mater.*, vol. 36,

no. 4, pp. 491–500, 2020, doi: 10.1016/j.dental.2020.01.017.
[48] V. Lughi and V. Sergo, “Low temperature degradation -aging- of zirconia: A critical review of the relevant aspects in dentistry.,” *Dent. Mater.*, vol. 26, no. 8, pp. 807–20, Aug. 2010, doi: 10.1016/j.dental.2010.04.006.
[49] R. C. Garvie, “The Occurrence of Metastable Tetragonal Zirconia as a Crystallite Size Effect,” *J. Phys. Chem.*, vol. 69, no. 4, pp. 1238–1243, 1965.
[50] F. F. Lange, “Transformation-Toughened Zr02: Correlations between Grain Size Control and Composition in the System,” *J. Am. Ceram. Soc.*, vol. 69, no. 3, pp. 240–242, 1986.
[51] A. G. Evans, N. Burlingame, M. Drory, and W. M. Kriven, “Martensitic transformations in zirconia- particle size effects and toughening,” vol. 29, 1981.
[52] R. C. Garvie, “Stabilization of the Tetragonal Structure in Zirconia Microcrystals,” *J. Phys. Chem.*, vol. 82, no. 2, pp. 218–224, 1978.
[53] N. Wu, T. Wu, and I. A. Rusakova, “Thermodynamic stability of tetragonal zirconia nanocrystallites,” *J. Mater. Res.*, vol. 16, no. 4, pp. 2–5, 2001.
[54] F. Zhang *et al.*, “Critical influence of alumina content on the low temperature degradation of 2-3mol% yttria-stabilized TZP for dental restorations,” *J. Eur. Ceram. Soc.*, vol. 35, no. 2, pp. 741–750, 2015, doi: 10.1016/j.jeurceramsoc.2014.09.018.
[55] A. Samodurova, A. Kocjan, M. V Swain, and T. Kosmač, “The combined effect of alumina and silica co-doping on the ageing resistance of 3Y-TZP bioceramics,” *Acta Biomater.*, vol. 11, pp. 477–487, 2015, doi: 10.1016/j.actbio.2014.09.009.
[56] I. M. Ross, W. M. Rainforth, D. W. Mccomb, and A. J. Scott, “The role of trace additions of alumina to yttria - tetragonal zirconia polycrystals (Y - TZP),” *Scr. Mater.*, vol. 45, pp. 653–660, 2001.
[57] X. Guo, “Low temperature degradation mechanism of tetragonal zirconia ceramics in water: role of oxygen vacancies,” *Solid State Ionics*, vol. 112, no. 1–2, pp. 113–116, 1998, doi: 10.1016/S0167-2738(98)00212-4.
[58] X. Guo, “Size dependent grain-boundary conductivity in doped zirconia,” *Comput. Mater. Sci.*, vol. 20, pp. 168–176, 2001.
[59] X. Guo and T. Schober, “Water Incorporation in Tetragonal Zirconia,” *J. Am. Ceram. Soc.*, vol. 87, no. 4, pp. 746–748, 2004, doi: 10.1111/j.1551-2916.2004.00746.x.
[60] T. Duong, A. M. Limarga, and D. R. Clarke, “Diffusion of water species in yttria-stabilized zirconia,” *J. Am. Ceram. Soc.*, vol. 92, no. 11, pp. 2731–2737, 2009, doi: 10.1111/j.1551-2916.2009.03271.x.